Inorganic Chemistry

Article

Cite This: Inorg. Chem. XXXX, XXX, XXX−XXX

pubs.acs.org/IC

Copper(II) Complexes with Bulky N-Substituted Diethanolamines: High-Field Electron Paramagnetic Resonance, Magnetic, and Catalytic Studies in Oxidative Cyclohexane Amidation

Oksana V. Nesterova,[†] Dmytro S. Nesterov,*[,†] Julia Jezierska,[‡] Armando J. L. Pombeiro,*[,†] and Andrew Ozarowski[§]

[†]Centro de Química Estrutural, Instituto Superior Técnico, Universidade de Lisboa, Av. Rovisco Pais, 1049-001 Lisboa, Portugal
[‡]Faculty of Chemistry, University of Wroclaw, 14 Joliot-Curie Str., 50-383, Wroclaw, Poland
[§]National High Magnetic Field Laboratory, Florida State University, 1800 East Paul Dirac Drive, Tallahassee, Florida 32310, United States

Supporting Information

ABSTRACT: The novel coordination compounds $[Cu_2(H^tBuDea)_2(OAc)_2]$ (**1**) and $[Cu_2(H^nBuDea)_2Cl_2]\cdot nH_2O$ (**2**) have been prepared through the reaction of the respective copper(II) salts with *N-tert*-butyldiethanolamine ($H_2{}^tBuDea$, for **1**) or *N*-butyldiethanolamine ($H_2{}^nBuDea$, for **2**) in methanol solution. Crystallographic analysis reveals that, in spite of the common binuclear $\{Cu_2(\mu\text{-}O)_2\}$ core, the supramolecular structures of the complexes are drastically different. In **1** binuclear molecules are linked together by H-bonds into 1D chains, while in **2** the neighboring pairs of binuclear molecules are H-bonded, forming tetranuclear aggregates. Variable-temperature (1.8−300 K) magnetic susceptibility measurements of **1** and **2** show a dominant antiferromagnetic behavior. Both complexes are also studied by HF-EPR spectroscopy. While the interaction between Cu(II) centers in **1** can be described by a single coupling constant J = 130.1(3) cm^{-1} (using $H = JS_1S_2$), the crystallographically different $\{Cu_2(\mu\text{-}O)_2\}$ pairs in **2** are expected exchange from ferro- to antiferromagnetic behavior (with J ranging from −32 to 110 cm^{-1}, according to DFT calculations). Complexes **1** and **2** act as catalysts in the amidation of cyclohexane with benzamide, employing $^tBuOO^tBu$ as oxidant. The maximum achieved conversion of benzamide (20%, after 24 h reaction time) was observed in the $1/{}^tBuOO^tBu$ system. In the cases of $^tBuOO(O)CPh$ or ^tBuOOH oxidants, no significant amidation product was observed, while for $^tBuOO(O)CPh$, the oxidative dehydrogenation of cyclohexane occurred, giving cyclohexene, to afford the allylic ester (cyclohex-2-en-1-yl benzoate) as the main reaction product.

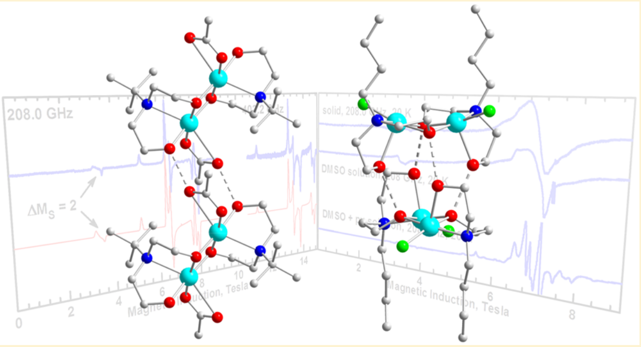

INTRODUCTION

Aliphatic aminoalcohols are organic compounds that are broadly used for the construction of homo- and heterometallic molecular complexes, which are of continuing interest in modern chemistry.[1] Such ligands show often a tripodal coordination in a variety of metal complexes in which they do not readily dissociate from the metal center.[2] Moreover, in the majority of cases, these ligands facilitate the preparation of close-packed molecules[2,3] and therefore are able to form complexes with interesting magnetic properties,[4] such as single-molecule magnetism behavior, namely with copper.[5] Diethanolamines (H_2RDea) with an organic group (R) at the nitrogen atom belong to a broadly explored family of aliphatic aminoalcohol ligands.[1,6] Although the coordination chemistry of diethanolamines has a long history, the properties of such compounds substituted with bulky neutral (aliphatic) fragments are less studied, and almost unexplored for copper complexes. Recently we have shown that *N-tert*-butyldiethanolamine behaves as an efficient agent in stabilizing unique Cu8 paramagnetic clusters.[7,8] It was proposed that the bulky *tert*-butyl fragment promoted the formation and isolation of such a polynuclear architecture. On the other hand, we anticipate that these fragments may also facilitate the solubility of Cu(II) coordination compounds in nonpolar solvents, like benzene, toluene, or alkanes, which can be a crucial point in catalytic studies.

Copper complexes are of special importance in a broad range of catalytic reactions,[1,9−16] including the radical functionalization of inert alkanes, where an sp^3 C−H bond undergoes hydrogen abstraction to produce a carbon-centered alkyl radical.[17] Alkyl radicals are reactive species, readily reacting with amides,[18] amines,[19] arylborates,[20] carboxylic acids,[21,22] or aliphatic groups,[23] providing a powerful tool for

Received: July 29, 2018

DOI: 10.1021/acs.inorgchem.8b02145

Scheme 1. Schematic Representations of the Structures of Complexes 1 and 2, as Well as Their Syntheses

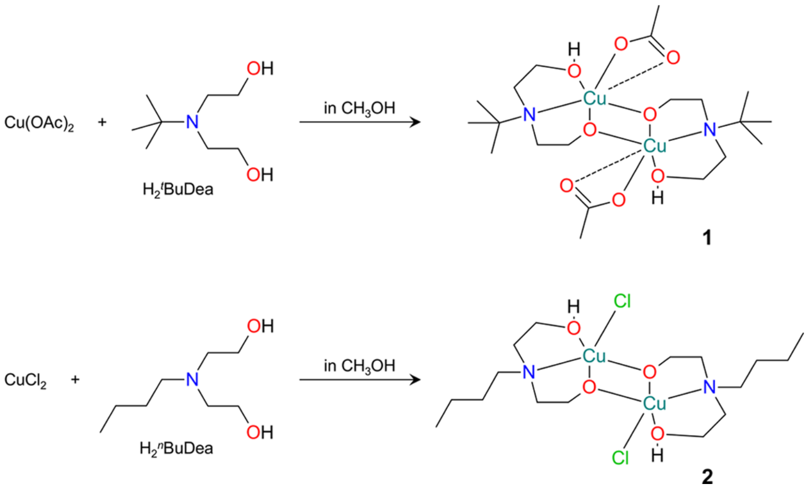

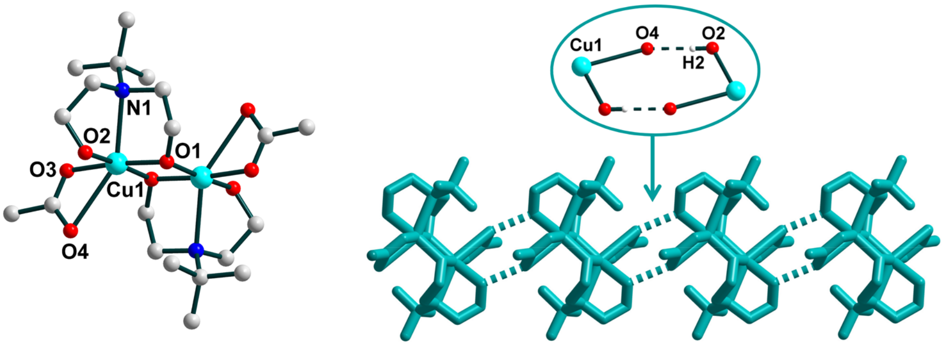

Figure 1. (Left) Crystal structure of **1**, showing the atom numbering. H atoms are omitted for clarity. Color scheme: Cu, cyan; O, red; N, blue; C, gray. (Right) Representation of the supramolecular chain in **1** with the enlarged fragment showing H-bonding interactions between bimetallic units. The hydrogen atoms are omitted for clarity.

organic synthesis. However, the study of such catalytic processes, being typically catalyzed by complexes of copper or iron, is still rather limited and has been hampered by solubility restrictions in suitable solvents. Considering the recognized activity of aminoalcohol copper complexes in radical oxidation of alkanes with peroxides in polar solvents (acetonitrile/water),[1,9] we propose *N*- and *tert*-butyldiethanolamines, with a relevant organic group, as suitable ligands for radical alkane functionalization: while the bulky aliphatic fragment provides solubility of the complex in a desired nonpolar solvent, the diethanolamine moiety supports the catalytically active copper species in solution. Herein we report synthetic and structural features, magnetic, high-field electron paramagnetic resonance (HF-EPR)/density functional theory (DFT) characterization, and catalytic properties in cyclohexane amidation in a nonpolar solvent (benzene) of the novel binuclear complexes $[Cu_2(H^tBuDea)_2(OAc)_2]$ (**1**) and $[Cu_2(H^nBuDea)_2Cl_2]\cdot nH_2O$ (n = 0.037 or 0.5) (**2**) (Scheme 1).

■ RESULTS AND DISCUSSION

Synthesis and IR Characterization. Compounds **1** and **2** are formed through the reaction of a copper(II) salt (acetate for **1** and chloride for **2**) with *N*-*tert*-butyldiethanolamine ($H_2{}^tBuDea$, for **1**) or *N*-butyldiethanolamine ($H_2{}^nBuDea$, for **2**) in methanol solutions, using the molar ratio of CuX$_2$:L = 1:2. Both reactions were initiated and brought to completion by heating and stirring in open air. In the case of **1**, precipitation of the main product occurred in a few minutes after the initiation of the reaction. After 40 min, the reaction was stopped and the product was filtered off. Light-blue microcrystals of **1** suitable for the X-ray crystallographic study were formed in 2 days from the filtrate without any additional procedures. For **2**, precipitation was also observed immediately after the start of the reaction, but during the reaction time (1 h) the formed powder was completely dissolved, and a clear green-blue solution was obtained. This solution was filtered, and green crystals of **2** suitable for X-ray crystallographic study (see next section) were formed in 1 day. The general reactions for the synthesis of **1** and **2** are expressed by eqs 1 and 2.

$$2Cu(OAc)_2\cdot H_2O + 2H_2{}^tBuDea \rightarrow [Cu_2(H^tBuDea)_2(OAc)_2] + 2HOAc + 2H_2O \qquad (1)$$

$$2CuCl_2\cdot 2H_2O + 2H_2{}^nBuDea \rightarrow [Cu_2(H^nBuDea)_2Cl_2] + 2HCl + 4H_2O \qquad (2)$$

Compound **2** typically crystallizes with one molecule of water per four copper atoms, although we observed that in some cases (structure **2c**) the lattice may contain much smaller amounts of water. Thus, the final composition of the complex should be established by elemental or X-ray diffraction analysis data.

The IR spectra of **1** and **2** show complex patterns in the 400−2000 cm^{-1} region (Figure S1). Strong absorptions at

1564 and 1420 cm^{-1} in the spectrum of **1** can be associated with ν_a(COO) and ν_s(COO) vibrations of the coordinated acetate group.[24] The Δ value [ν_a(COO) − ν_s(COO)] of 144 cm^{-1} is in accord with the bidentate function of the acetate group.[25] Considering these spectra as the characteristic ones, we used them to monitor if the structures of **1** and **2** are retained after recrystallization from nonpolar solvents. Benzene was the solvent of primary interest (see below for the catalytic properties). While complex **1** is sparingly soluble in benzene, complex **2** dissolves, to some extent, even at room temperature. The IR spectra of compounds obtained after recrystallization reveal the identity of the compounds before and after dissolution in hot benzene for both **1** and **2** (Figure S2). Hence, we suppose that the structures of both complexes are retained during the recrystallization from benzene. Slow evaporation of a benzene solution of **2** afforded a crystalline material which was subjected to single-crystal X-ray analysis. The structure of the recrystallized species from benzene was not solved due to poor crystal quality and probable twinning problem (space group C_2 was observed, instead of $P2/c$ for the un-recrystallized **2**), but it was possible to see the dimeric copper fragments with a Cu···Cu separation of 2.956 Å.

Crystal Structures. The single-crystal X-ray analysis reveals that [$Cu_2(H^tBuDea)_2(OAc)_2$] (**1**) is based on a centrosymmetric binuclear {$Cu_2(\mu\text{-}O)_2$} core (Figure 1, left). The complex molecules are linked together by strong hydrogen-bonding, forming extended supramolecular chains (Figure 1, right).

In the crystal structure of **1**, the *N-tert*-butyldiethanolaminate ligands are monodeprotonated and show tridentate (O,N,O) coordination, accounting for the formation of the molecular-type structure and for partial compensation of the metal ion charge. The copper(II) ions in **1** have distorted octahedral coordination environments, with an O_5N donor set formed by oxygen and nitrogen atoms from tripodal *N-tert*-butyldiethanolamine and bidentate-chelating acetate ligands. The equatorial Cu−O distances lie in the range from 1.9248(14) to 2.0313(16) Å, while apical Cu−O/N bond lengths are 2.4960(17) and 2.7418(16) Å (Table S1). The *cis* and *trans* O−Cu−O(N) bond angles vary from 53.03(5) to 122.14(5)° and from 149.22(5) to 174.14(6)°, respectively. Such a deviation of the coordination geometry from a regular octahedron is mainly caused by the asymmetric coordination of the bidentate-chelating acetate ligands [$\text{Cu−O3}_{\text{OAc}}$ = 1.9528(15) Å and $\text{Cu−O4}_{\text{OAc}}$ = 2.7418(16) Å], which are also involved in the formation of strong hydrogen bonds using the weakly coordinated O4 atom. In the binuclear complex the Cu···Cu distance is 2.9471(6) Å.

The strong H-bonds, O—H···O, involving oxygen atoms from asymmetric bidentate-chelating acetate and tridentate H^tBuDea^- ligands (Table 1), are responsible for the formation of the overall 1D structure (Figure 1, right), where the eight-membered {$Cu_2O_2(OH)_2$} supramolecular synthons (Figure 1, right, in the circle) play the role of chain-building fragments. Further increase of the dimensionality of the H-bonded polymer is not possible due to steric factors: the *N-tert*-butyl groups of the aminoalcohol ligands prevent the formation of hydrogen bonds between adjacent chains (Figure S3). The shortest Cu···Cu separation within the supramolecular chain is 6.10 Å.

The crystal structure of [$Cu_2(H^nBuDea)_2Cl_2$]·$n$$H_2O$ (**2**) (Figure 2, left) is based, as for **1**, on the same binuclear {$Cu_2(\mu\text{-}O)_2$} core, but in the case of **2** the neighboring pairs of binuclear molecules are H-bonded together, forming tetranuclear supramolecular aggregates (Figure 2, right). Depending on the crystallization conditions, the complex **2** may contain up to one water molecule per four copper dimers. The crystal structure of **2** has been made in triplicate (see the Experimental Section), showing n = 0.5 (for **2a** and **2b**) or 0.037 (for **2c**). A similar motif with *N*-propyldiethanolamine ($H_2PrpDea$) was found earlier for the binuclear complex [$Cu_2(HPrpDea)Cl_2$].[26]

Table 1. Geometrical Parameters of H-Bonding in 1 and 2

compd	H-bond	d(O···O), Å	d(O−H), Å	∠(O−H···O), deg
1	O2—H2···O4[a]	2.563(2)	0.77(3)	175(4)
2a	O101—H1···O302[b]	2.679(6)	0.84(2)	172(7)
	O301—H3···O102	2.704(6)	0.85(2)	169(6)
	O401—H4···O202	2.673(6)	0.85(2)	160(6)
	O201—H2···O402[c]	2.693(6)	0.85(2)	169(7)
2b	O101—H1···O302[b]	2.683(4)	0.72(4)	172(5)
	O301—H3···O102	2.709(4)	0.77(4)	168(5)
	O401—H4···O202	2.678(4)	0.82(4)	170(4)
	O201—H2···O402[c]	2.694(4)	0.65(4)	173(6)
2c	O101—H1···O302[b]	2.695(3)	0.65(3)	172(4)
	O301—H3···O102	2.729(3)	0.72(3)	176(3)
	O401—H4···O202	2.691(3)	0.62(3)	178(4)
	O201—H2···O402[c]	2.707(3)	0.73(3)	171(3)

[a] 3 − x, 2 − y, −z. [b] 2 − x, y, 1/2 − z. [c] 1 − x, y, 1/2 − z.

Similar to the *N-tert*-butyldiethanolamines in **1**, the *N*-butyldiethanolamine ligands in **2** are monodeprotonated and show the tripodal tridentate (O,N,O) coordination mode. The overall crystal structure of the complex **2** consists of four crystallographically independent molecules, where all copper(II) atoms are five-coordinated. The O_3NCl donor sets around Cu1, Cu2, Cu3, and Cu4 atoms are formed by two oxygen atoms and one nitrogen atom from aminoalcohol ligands and a coordinated chlorine atom [Cu−O(N,Cl) = 1.941(4)−2.2269(14) Å, Table S2] in the equatorial plane, and one oxygen atom from the H^nBuDea^- ligand [$\text{Cu−O}_{\text{HBuDea}^-}$ = 2.277(3)−2.296(2) Å for O101; 2.288(3)−2.300(4) Å for O201; 2.291(3)−2.304(4) Å for O301; 2.292(3)−2.320(2) Å for O401] at the apical position. The *cis* and *trans* O−Cu−O(N, Cl) bond angles vary from 79.02(16) to 103.65(7)° and from 163.29(18) to 168.92(9)°, respectively (Table S3). In the binuclear complexes, the Cu···Cu distances for **2a**−**2c** are in the ranges 2.9194(9)−2.9271(6) Å (for Cu1···Cu1), 2.9713(9)−2.9774(6) Å (for Cu2···Cu2), 2.9459(13)−2.9498(5) Å (for Cu3···Cu3), and 2.9599(10)−2.9637(6) Å (for Cu4···Cu4) (Table S2).

The binuclear molecules are joined together pairwise by a set of strong O−H···O hydrogen bonds, involving all oxygen atoms from both bimetallic parts (Table 1). Thereby, two

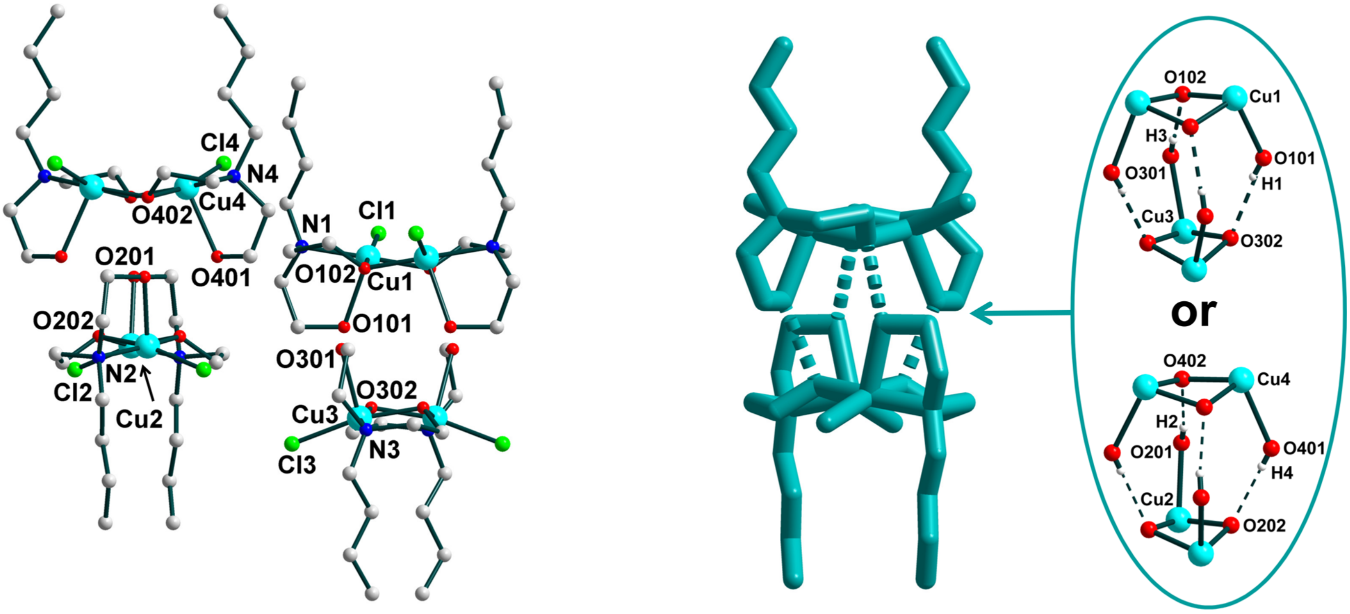

Figure 2. (Left) Crystal structure of the main structure of **2**, showing the atom numbering. The uncoordinated water molecule and H atoms are omitted for clarity. Color scheme: Cu, cyan; O, red; N, blue; C, gray. (Right) Representation of the supramolecular tetrametallic units based on atoms Cu1/Cu3 and Cu2/Cu4, and detail showing H-bonding interactions with atom numbering.

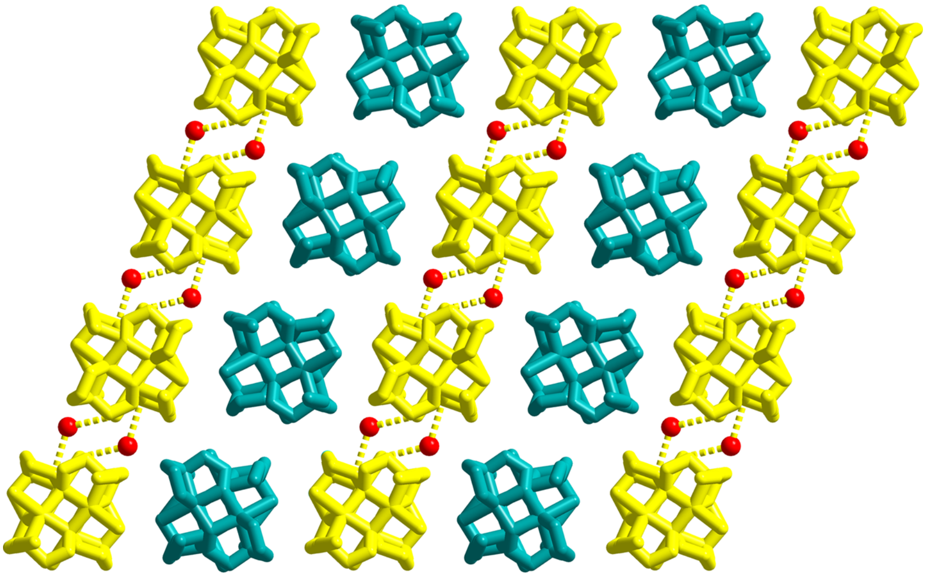

Figure 3. Representation of the packing in **2** viewed down the *b* axis.

crystallographically independent tetranuclear supramolecular aggregates are formed: one of them is based on the Cu1/Cu3 atom pair and the second one on Cu2/Cu4 (Figure 2, right). In both cases the determinant supramolecular synthon that accounts for such a type of structure formation is more complicated than in the structure of **1** and consists of four supramolecular eight-membered $\{Cu_2O_2(OH)_2\}$ rings joined with two $\{Cu_2(\mu\text{-}O)_2\}_2$ parts, involving, in general, four copper(II) and eight oxygen atoms (Figure 2, right). The obtained tetranuclear aggregates reveal the "key-lock" basis of the assembly, where the copper(II) atoms are located at a vertexes of a distorted tetrahedron.

Formation of a complicated supramolecular structure with participation of all tetranuclear units and solvate water molecules is hampered by the presence of bulky *N*-butyl groups of the aminoalcohol ligands, which sterically prevent H-bonding between neighboring tetranuclear aggregates (Figure S4). However, within the crystal structure packing, the supramolecular tetranuclear aggregates based on Cu1/Cu3 atom pairs are H-bonded to the solvate H_2O molecules, forming supramolecular polymeric chains (Figure 3, yellow motifs) between which tetranuclear units based on Cu2/Cu4 pairs are located (Figure 3, blue motifs).

Magnetic Properties of 1. The dependence of the effective magnetic moment (μ_{eff}) on the temperature for the binuclear complex **1** (Figure 4) is indicative of antiferromagnetic exchange within the copper dimeric units. The experimental data can be successfully fitted using the Bleaney—Bowers equation, eq 3 (spin Hamiltonian $H = JS_1S_2$), to get the best fit values of $g = 2.02(1)$, $J = 130.1(3)$ cm^{-1}, $\rho = 0.0014(1)$,

DOI: 10.1021/acs.inorgchem.8b02145
Inorg. Chem. XXXX, XXX, XXX−XXX

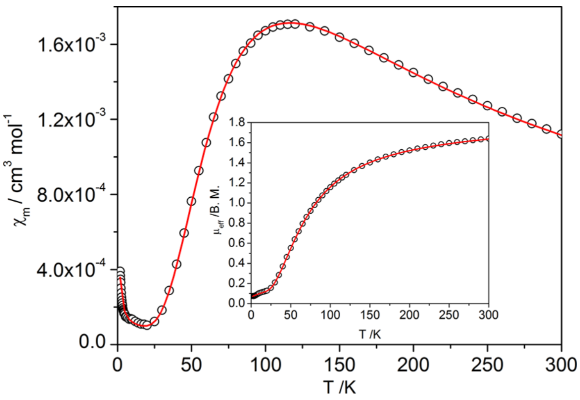

Figure 4. Dependences of the molar magnetic susceptibility (main plot) and effective magnetic moment (inset) on the temperature for **1**. Open circles are experimental data related to one copper atom; solid lines are theoretical fits using $g = 2.02(1)$, $J = 130.1(3)$ cm^{-1}, $\rho = 0.0014(1)$, and TIP = 67(4) × 10^{-6} cm^3 mol^{-1}.

and TIP = 67(4) × 10^{-6} cm^3 mol^{-1}, where ρ is the paramagnetic impurity fraction and TIP is the temperature-independent paramagnetism. The magnitude of TIP, obtained from the fitting of experimental data, is close to that expected (60 × 10^{-6} cm^3 mol^{-1}) for a Cu$^{\text{II}}$ ion. The sign of exchange coupling constant J is in agreement with the relatively large Cu−O−Cu angle of 99.3°.[27] Antiferromagnetic interactions are expected in systems like **1** when the CuOCu angle exceeds 97°.

$$\chi = \frac{Ng^2\beta^2}{3kT}\frac{3e^{-J/kT}}{1 + 3e^{-J/kT}}(1 - \rho) + \frac{Ng^2\beta^2}{3kT}\frac{3}{4}\rho + \text{TIP} \tag{3}$$

Solid-State EPR Spectra of 1. Relatively strong exchange interactions between two $S = {}^1/_2$ Cu^{2+} ions in **1** result in an $S = 0$ ground state and a thermally accessible $S = 1$ excited state which is EPR active. A standard spin Hamiltonian for $S = 1$ was therefore used in simulations of the powder spectra:

$$\hat{\mathbf{H}} = \mu_{\text{B}}\mathbf{B}\{\mathbf{g}\}\hat{\mathbf{S}} + D\left\{\hat{\mathbf{S}}_z^2 - \frac{1}{3}S(S+1)\right\} + E(\hat{\mathbf{S}}_x^2 - \hat{\mathbf{S}}_y^2) \tag{4}$$

Not surprisingly, complex **1** exhibits EPR spectra similar to those of other Cu^{2+} dimers with alkoxo bridges of a similar structure. Simulation procedures led to the parameter set $g_x = g_y = 2.063$, $g_z = 2.337$, $D = -1.327$ cm^{-1}, $E = -0.065$ cm^{-1}. A characteristic feature of such systems is that the **g**-matrix and zero-field-splitting tensor must be assumed non-coaxial for a successful simulation. In previous papers by some of us, a tilting angle of 11° between the g_z and D_{zz} directions was found.[28,29] In the present case, the spectra shown in Figure 5 were simulated with a tilting angle of 10°. The sign of D could not be determined from the powder EPR spectra of the present antiferromagnetic complex, but it was found to be negative in both ferro- and antiferromagnetic dimers with a similar CuOOCu bridge arrangement.[28,29] We will assume that D is negative also in our case.

With the Cu···Cu distance of 2.947 Å, the contribution of the magnetic dipolar interactions to the zero-field-splitting tensor is as follows (x is the Cu−Cu direction, z is perpendicular to CuOOCu plane):

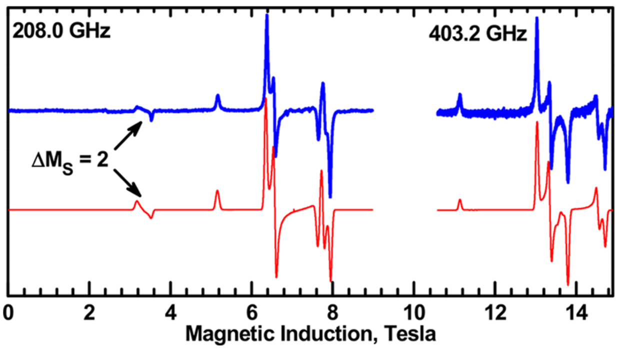

Figure 5. HF-EPR spectra of **1** recorded at 80 K with the microwave frequencies as indicated. Blue: experimental; red: simulated using $g_x = g_y = 2.063$, $g_z = 2.337$, $D = -1.327$ cm^{-1}, $E = -0.065$ cm^{-1}.

$$\begin{aligned} D_{xx}^{\text{dipole}} &= -g_x^{\,2}\mu_{\text{B}}^{\,2}/R_{\text{Cu-Cu}}^3 = -0.072 \text{ cm}^{-1} \\ D_{yy}^{\text{dipole}} &= g_y^{\,2}\mu_{\text{B}}^{\,2}/2R_{\text{Cu-Cu}}^3 = 0.036 \text{ cm}^{-1} \\ D_{zz}^{\text{dipole}} &= g_z^{\,2}\mu_{\text{B}}^{\,2}/2R_{\text{Cu-Cu}}^3 = 0.046 \text{ cm}^{-1} \end{aligned} \tag{5}$$

From the experimental spin Hamiltonian parameter set $D = -1.327$ cm^{-1}, $E = -0.065$ cm^{-1}, one can get the diagonal elements of the zero-field-splitting tensor $\{\mathbf{D}\}$:

$$\begin{aligned} D_{xx} &= -D/3 + E = 0.377 \text{ cm}^{-1} \\ D_{yy} &= -D/3 - E = 0.507 \text{ cm}^{-1} \\ D_{zz} &= 2D/3 = -0.885 \text{ cm}^{-1} \end{aligned}$$

The experimental $\{\mathbf{D}\}$ tensor is the sum of the dipolar and exchange-related contributions,

$$\{\mathbf{D}\} = \{\mathbf{D}^{\text{dipolar}}\} + \{\mathbf{D}^{\text{exchange}}\} \tag{6}$$

The diagonal elements of $\{\mathbf{D}^{\text{exchange}}\}$ can thus be calculated from $D_{xx}^{\text{ex}} = D_{xx} - D_{xx}^{\text{dipole}}$, etc.:

$$D_{xx}^{\text{ex}} = 0.449 \text{ cm}^{-1}, \quad D_{yy}^{\text{ex}} = 0.471 \text{ cm}^{-1},$$
$$D_{zz}^{\text{ex}} = -0.931 \text{ cm}^{-1}$$

From these diagonal elements, the scalar parameters $D^{\text{ex}} = -1.39$ cm^{-1} and $E^{\text{ex}} = -0.011$ cm^{-1} are found from

$$D = (2D_{zz} - D_{xx} - D_{yy})/2, \qquad E = (D_{xx} - D_{yy})/2 \tag{7}$$

The superscript "ex" has been omitted because relations (7) are valid for all tensors under discussion, that is, $\{\mathbf{D}\}$, $\{\mathbf{D}^{\text{exchange}}\}$, and $\{\mathbf{D}^{\text{dipolar}}\}$.

It is seen that the zero-field-splitting tensor is mainly exchange-related and is remarkably axial, meaning that D_{xx}^{ex} is close to D_{yy}^{ex} (or $|E_{\text{ex}}| \ll |D_{\text{ex}}|$).

The theory of the exchange-related zero-field splitting has been formulated for the well-known dimeric "paddlewheel" copper(II) carboxylates, in which Cu(II) has the $d_{x^2-y^2}$ ground state, like in our complex.[30−33]

The exchange interaction anisotropy is caused by mixing of the excited states of a system with its ground state via spin−orbit coupling. In such excited dimer states, one of the copper ions remains in its ground state $d_{x^2-y^2}$, while another Cu is promoted to one of its excited states. Additionally, a non-zero matrix element of the **L** operator must exist between that excited state and the ground state. D_{ex} and E_{ex} can be expressed as[30−33]

$$D^{ex} = 2\frac{\lambda^2 J_{x^2-y^2,xy}}{\Delta E^2_{x^2-y^2,xy}} - \frac{1}{4}\frac{\lambda^2 J_{x^2-y^2,xz}}{\Delta E^2_{x^2-y^2,xz}} - \frac{1}{4}\frac{\lambda^2 J_{x^2-y^2,yz}}{\Delta E^2_{x^2-y^2,yz}}$$

$$E^{ex} = \frac{1}{4}\frac{\lambda^2 J_{x^2-y^2,xz}}{\Delta E^2_{x^2-y^2,xz}} - \frac{1}{4}\frac{\lambda^2 J_{x^2-y^2,yz}}{\Delta E^2_{x^2-y^2,yz}} \qquad (8)$$

Symbols $J_{x^2-y^2,n}$ represent the exchange integrals between the ground state of one copper ion and an excited state of another. λ is the spin−orbit coupling constant, which equals −828 cm^{-1} for a free Cu^{2+} ion but in a complex may be substantially reduced by the covalency effects. Figure 6 shows that the interactions $d_{x^2-y^2}$−d_{xz} and $d_{x^2-y^2}$−d_{yz} are expected to be of similar magnitudes. The formulas for D^{ex} and E^{ex} involve the same quantities $\lambda/\Delta E(d_{x^2-y^2},d_n)$ which appear in the theory of g of Cu^{2+}:

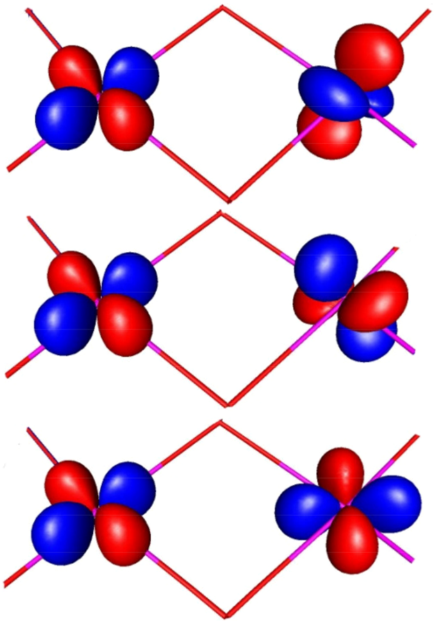

Figure 6. Arrangement of the $d_{x^2-y^2}$ orbital of a Cu^{2+} ion (left) versus the excited orbitals d_{xz}, d_{yz}, and d_{xy} (right top, center, and bottom, respectively) in a CuOOCu bridge. The z-axis is perpendicular to CuOOCu. The interactions $d_{x^2-y^2}$−d_{xz} and $d_{x^2-y^2}$−d_{yz} are expected to be of similar magnitudes.

$$g_z = 2.0023 - \frac{8\lambda}{\Delta E_{x^2-y^2,xy}}$$

$$g_{x(y)} = 2.0023 - \frac{2\lambda}{\Delta E_{x^2-y^2,yz(xz)}} \qquad (9)$$

Since $g_x = g_y$ in our complex, the expressions $\lambda/\Delta E(d_{x^2-y^2},d_{yz})$ and $\lambda/\Delta E(d_{x^2-y^2},d_{xz})$ must also be of similar magnitudes, and so must be the two $\{\mathbf{D}^{exchange}\}$ tensor components, whose difference appears in eq 8 for E^{ex}. Accordingly, E^{ex} is expected to be small, as observed. Theory predicts that the **g**-matrix in a centrosymmetric dimer should be coaxial with the $\{\mathbf{D}^{exchange}\}$ tensor.[30−32] The experimental results presented here show that this is not exactly the case, as the tilting angle of 10° between the total zero-field splitting, that is, $\{\mathbf{D}^{dipolar}\} + \{\mathbf{D}^{exchange}\}$, and the **g** direction is observed. Interestingly, this non-coaxiality is observed in all complexes with the $Cu(OR)_2Cu$ bridges,[17,18] including $Cu(OH)_2Cu$.[33] Neglecting this small but visible effect, we can summarize that the dipolar contribution to the zero-field-splitting tensor is axial about the Cu−Cu direction, while the contribution due to the anisotropic exchange is axial about the direction approximately perpendicular to the CuOOCu plane. Their sum is therefore non-axial, resulting in the experimental E parameter of −0.065 cm^{-1}. While E is much smaller than D, it is much larger than that observed in the "paddlewheel" copper carboxylates, in which both the dipolar and exchange contributions are axial about the Cu−Cu direction.

Frozen Solution EPR Spectra of 1. Since the catalysis occurs in solution, a question arises whether the compound retains its dimeric structure therein. The solubility of **1** in benzene or toluene was insufficient for preparing good frozen solution samples. We found that **1** dissolves sufficiently in $CHCl_3$ and in CH_2Cl_2, and frozen solution spectra were taken in a 1:1 mixture of these solvents. The solvent mixture was used to improve the glass quality, as pure solvents tend to freeze into a crystalline "ice", producing bad EPR spectra. At 80 K, a characteristic $S = 1$ spectrum was seen with the D and E parameters different from those observed in the solid at 80 K (Figure 7).

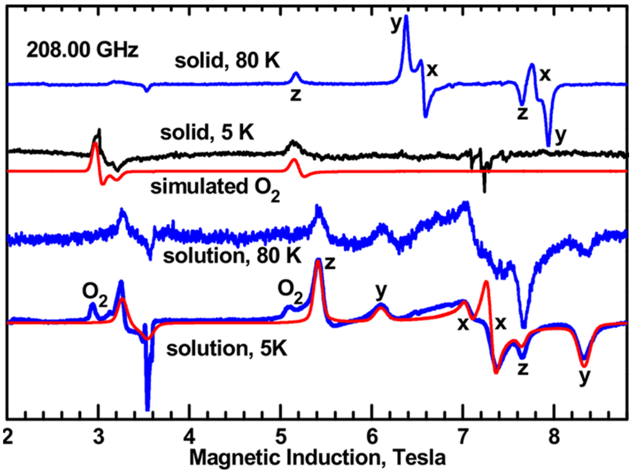

Figure 7. HF-EPR spectra recorded with 208 GHz for the solid **1** and its frozen solution at the temperatures indicated. The solution spectrum at 5 K was simulated with $g_x = g_y = 2.055$, $g_z = 2.273$, $D = -1.187$ cm^{-1}, $E = -0.318$ cm^{-1} (red trace at the bottom). Opposite to the spectrum of the solid, no tilting of the $\{\mathbf{D}\}$ tensor versus g was required in simulations. Labels x, y, z indicate the molecular orientations at which the observed resonances occur. Resonances labeled O_2 are due to oxygen adsorbed on the sample, and a simulated spectrum of O_2 ($S = 1$, $g_{xyz} = 2$, $D = 3.571$ cm^{-1}, $E = 0$) is shown as the upper red trace.

Moreover, that spectrum persisted down to 5 K, while solid samples exhibited at 5 K only signals due to monomeric impurities plus a signal due to molecular oxygen adsorbed on the sample. The $S = 1$ state spectrum of the copper dimer was suppressed due to strong antiferromagnetic interactions in solid **1**. It is thus clear that the sign of J has changed, or at least the antiferromagnetic interaction was very substantially reduced. As far as the zero-field-splitting parameters are concerned, there is 11% reduction of D from −1.327 cm^{-1} in the solid to −1.187 cm^{-1} in solution. The negative sign of D in solution has been experimentally determined (while it had to be assumed in the solid state). Negative and positive D produce very different intensity patterns in spectra simulated at 5 K, and only negative D is consistent with the 5 K spectrum in Figure 7. Much more pronounced is the change in E, from -0.065 to -0.318 cm^{-1}. The molecular geometry of the dimer must therefore have changed. The CuOCu angle in the solid **1** is 99.3° and squeezing it down to ~97° should result in a ferromagnetic interaction.[27] The E parameter as large as -0.3 cm^{-1} cannot be due to the dipolar interactions between the two copper ions. The drastic increase in E must therefore be due to the anisotropic exchange interactions. According to formulas (8), splitting of the energies of the xz and yz orbitals would produce non-zero E^{ex}. However, this must be rejected, as g_x remains equal to g_y (see formulas (9)). Presumably, a lowering of the CuOOCu bridge symmetry causes differentiation of the $d_{x^2-y^2}-d_{xz}$ and $d_{x^2-y^2}-d_{yz}$ interactions depicted in Figure 6. This will result in non-zero E^{ex} according to formulas (8). It is worth emphasizing that **1** recrystallized from a CH_2Cl_2+$CHCl_3$ solution exhibits in solid state again spectra shown in Figure 5.

In a series of $[Cu_2(RCOO)_2(H_2TEA)_2]$ complexes,[28] some species were relatively strongly ferromagnetic, while one was relatively strongly antiferromagnetic. The zero-field-splitting parameters D and E of the ferromagnetic and antiferromagnetic compounds were found to be not very different (and similar to the parameters of **1**). A similar effect may be observed in the present work—presumably small structural changes result in formation of ferromagnetic dimers in solution, but the zero-field splitting remains similar to that observed in the antiferromagnetic complex **1**. It should be emphasized that there is no proportionality between D and J, as the magnitude of J is determined by the interactions between the ground-state $d_{x^2-y^2}$ orbitals of two Cu^{2+} ions, while the zero-field splitting is associated with the exchange interactions in excited states; see formulas (8) and Figure 6 above.

Magnetic Properties of 2. The magnetic properties of **2** (Figures 8 and S5) appear to be non-interpretable. The system contains four crystallographically different dimers (Figure 2), and as the DFT calculations demonstrate (see below, Table 2), three of them are expected to be relatively strongly antiferromagnetic, with comparable coupling constants of 86–110 cm^{-1}, while one is very weakly antiferromagnetic, with J just 6 cm^{-1}, or even ferromagnetic, with $J = -32$ cm^{-1} (Table 2). Moreover, these four dimers in **2** are arranged into two different tetramers (Figure 2).

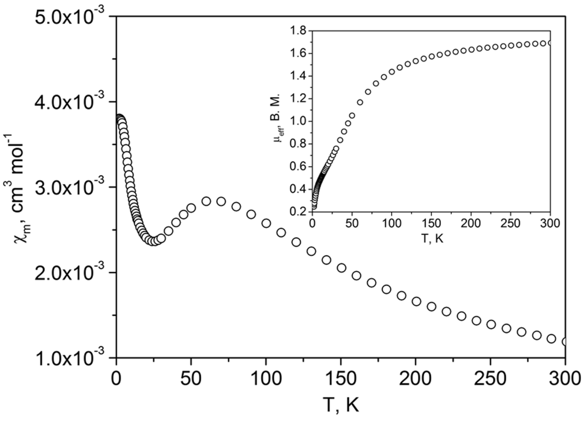

Figure 8. Dependences of the molar magnetic susceptibility (main plot) and effective magnetic moment (inset) on the temperature for **2c**. The data are recalculated per one copper atom.

Table 2. Inter-copper Distances, Cu–O–Cu Angles, and Calculated Exchange Coupling Constants for 1, 2a, and 2c

complex	copper pair	Cu···Cu distance, Å	Cu–O–Cu angle, °	J_{calc}, cm^{-1}
1	Cu1···Cu1	2.947	99.3	230
2a	Cu1···Cu1	2.921	96.3	−32
	Cu3···Cu3	2.945	97.1	58
	Cu4···Cu4	2.963	97.8	90
	Cu2···Cu2	2.971	98.0	74
2c	Cu1···Cu1	2.927	96.6	6
	Cu3···Cu3	2.950	97.6	86
	Cu4···Cu4	2.964	98.1	108
	Cu2···Cu2	2.977	98.3	110

Although the interdimer interactions in these tetramers are not expected to be strong, they are not vanishing, which may be inferred from EPR; no characteristic copper dimer spectra (like in **1**) were observed (Figure 9). The sample also shows the presence of monomeric impurities, and there are too many variables for a reliable fit. The higher temperature data ($T > 20$ K, Figure 8) indicate the presence of antiferromagnetic species with $J \approx 100$ cm^{-1}, but the entire curve cannot be fitted either by using the common model of a dimer plus monomeric impurity or by assuming one of the four dimers to be very weakly antiferromagnetic.

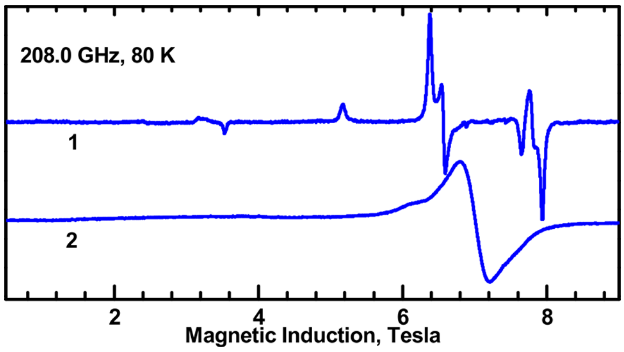

Figure 9. Comparison of the EPR spectra of solid **1** and **2** recorded at similar conditions.

The DFT calculations were also performed for the four different dimeric molecules present in complex **2**. The Cu–O–Cu angles in the dimers are close to the borderline (97–98°)[34,35] separating ferromagnetic and antiferromagnetic interactions in copper dinuclear systems. The calculations predict strong antiferromagnetic coupling in **1** and in three dimeric molecules present in **2**, while weak antiferromagnetic coupling is expected in the molecule with the smallest Cu–O–Cu angle of 96.3–96.6° and the shortest Cu···Cu distance (Table 2). This, however, cannot be reconciled with the magnetic susceptibility data.

Solid-State and Solution EPR Spectra of 2. Solid samples exhibit, at temperatures ~20 K and above, a featureless broad resonance centered at the effective g value of 2.11 (Figure 9). There is a shoulder on the low-field side of that broad band, which may be interpreted as a "parallel" $S = 1$ signal. The plot of the position of that shoulder versus the microwave frequency allows the estimate of $g_z = 2.25$ and $|D| = 0.51$ cm^{-1}, but there is no better evidence of the $S = 1$ spectra. Presumably, the weak interdimer and longer-range intermolecular exchange interactions blur the $S = 1$ spectra of dimers but are not sufficient to produce $S = 2$ spectra of the tetramers. The complex was dissolved in DMSO in a hope to reduce the interdimer interactions, and frozen solution spectra were recorded. The spectra indeed show at 5 K low-quality resonances coming from the $S = 1$ state with $g_z = 2.3$, $g_{xy} = 2.05$, and $D = -1.1$ cm^{-1}, thus similar to the parameters of **1** (Figure 10). The $\Delta M_S = 2$ resonances are clearly visible at ca. 3.2 T, but the entire spectrum cannot be simulated satisfactorily. It seems that the interdimer interactions were not eliminated in this solution. Finally, when a small amount of pyridine was added to the DMSO solution of **2**, complicated spectra indicating a mixture of monomeric, dimeric, and possibly tetrameric species were observed (Figure 10).

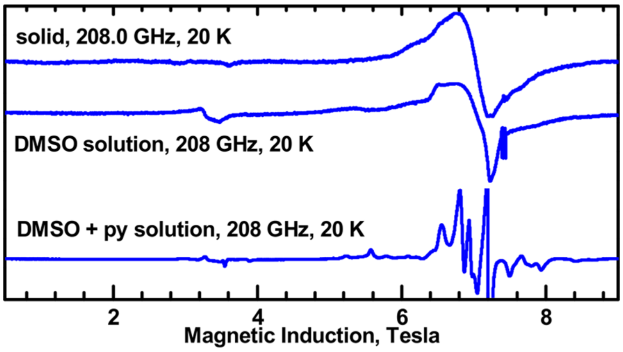

Figure 10. Spectra of **2** in solid state and in frozen solutions. The signal due to monomeric Cu^{2+} species in the bottom spectrum is cut off. The small feature at ~7.4 T in the two upper spectra is due to traces of Mn^{2+}.

A solution of **2** in DMSO+py stored for a longer time exhibits only monomeric species, with $g_{xy} = 2.06$ and $g_z = 2.27$. Some features in the spectra of fresh solutions indicate the presence of dimeric species (Figure 11). These spectra are observed at the lowest temperatures—down to 3 K; thus, the species are no longer antiferromagnetic, similarly to the observation in the frozen solution of **1**. Interestingly, the complicated spectrum observed in the frozen DMSO+py solution of **2** indicates also the presence of species larger than dimers.

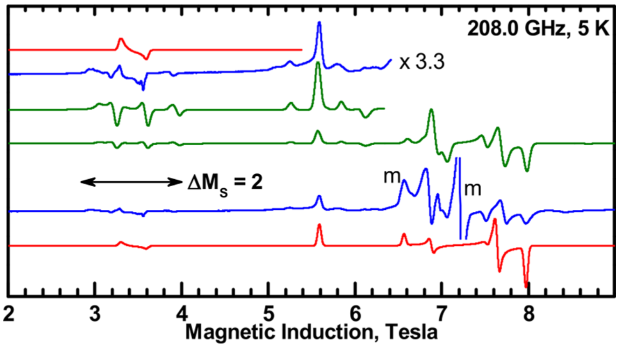

Figure 11. Blue: Frozen solution EPR spectrum of **2** dissolved in DMSO + pyridine. The signals attributed to a monomeric species with $g_z = 2.26$ and $g_{xy} = 2.05$ are designated by "m". A magnified part of the spectrum is also shown. The horizontal arrow indicates the $\Delta M_S = 2$ region. Red: Simulation assuming a dimer with $g_{xy} = 2.04$, $g_z = 2.265$, $D = -1.03$ cm^{-1}, $E = -0.093$ cm^{-1}. Green: Simulation using a model of two weakly interacting dimers (see text and SI).

Figure 11 shows an attempt to simulate that spectrum using a dimer model (red trace). It is seen that the $\Delta M_S = 2$ region cannot be reproduced due to the presence of satellite signals. Satellites are also present around a prominent transition at 5.6 T. Such signals may arise from weak interactions between two dimers. Since we have no information on the structure of such dimer pairs in solution, we will try to use the solid-state structure. If we number the copper ions so that 1 and 2 are part of one dimer and 3 and 4 belong to another one, the solid-state structure implies that there will be two strong (and assumed equal) interactions, 1−2 and 3−4. Interactions 1−3, 1−4, 2−3, and 2−4 are expected to be weak and are assumed all equal. It turns out that the magnitude of the latter ones determines the positions of the satellite lines seen in the spectrum in Figure 11. The calculation details are given in the SI. Simulations similar to that represented by the green lines in Figure 11 are obtained over a broad range of the intradimer interactions 1−2 and 3−4, both ferromagnetic and weakly antiferromagnetic. $J_{12} = J_{34} = -50$ cm^{-1} (ferromagnetic) was used in simulations. To obtain correct positions of the satellites of the strong "parallel" transition at 5.6 T, the isotropic interdimer interactions had to be assumed equal to -0.3 cm^{-1}. It appears thus possible that pairs of dimers are present in solutions of **2**, opposite to **1**, which does not exhibit intermolecular interactions in solution or in the solid state.

Catalytic Properties. Complexes **1** and **2** were tested as catalysts in the reaction of radical intermolecular amidation of inert C−H bonds of alkanes. The reaction of amidation of cyclohexane with benzamide, in benzene medium, was chosen as a model (Scheme 2).[18]

Scheme 2. Catalytic Amidation of Cyclohexane, Catalyzed by 1 and 2 (R = ^{t}Bu or H)

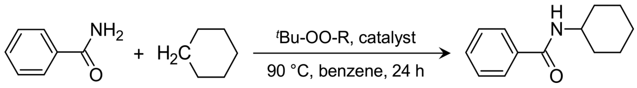

Complexes **1** and **2** contain bulky *tert*-butyl (**1**) and normal butyl (**2**) organic groups which facilitate their dissolution in the catalytic medium to achieve homogeneous reaction solutions. The reaction of 0.5 mmol of benzamide with 5 mmol of cyclohexane in the presence of 1 mmol of oxidant (^{t}BuOO^{t}Bu, di-*tert*-butylperoxide) and 12.5 μmol of catalyst (**1** or **2**, 2.5 mol% relative to benzamide) affords *N*-cyclohexylbenzamide (Scheme 2). The formation of this product was observed only when ^{t}BuOO^{t}Bu oxidant was used (Figure 12). Only traces of the target product were seen in the case of ^{t}BuOO(O)CPh (*tert*-butyl peroxybenzoate), while with ^{t}BuOOH no amidation product was detected. The maximum achieved conversion of benzamide (in the case of the **1**/^{t}BuOO^{t}Bu system) was 20% after 24 h reaction time. Fragments of chromatograms showing the characteristic peaks of products are depicted in Figure 12.

The **1**/^{t}BuOO^{t}Bu system was found to exhibit a higher activity than **2**/^{t}BuOO^{t}Bu (Figure 12). The latter also revealed chlorocyclohexane as a byproduct. A possible reason for chlorocyclohexane formation could be the competition

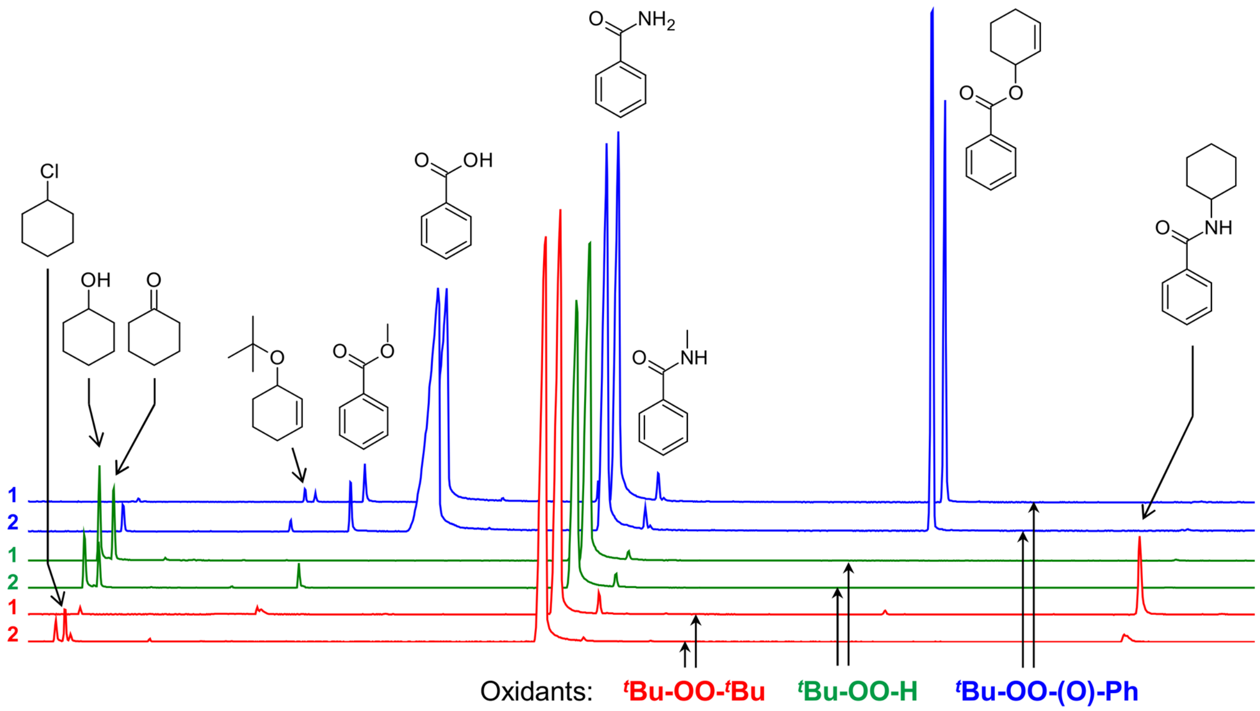

Figure 12. Fragments of the chromatograms showing the reaction products of amidation of cyclohexane with benzamide in the presence of the copper catalyst **1** or **2**. The initial parts of the chromatograms containing large peaks of benzene, cyclohexane, and *α*,*α*,*α*-trifluorotoluene are omitted for clarity.

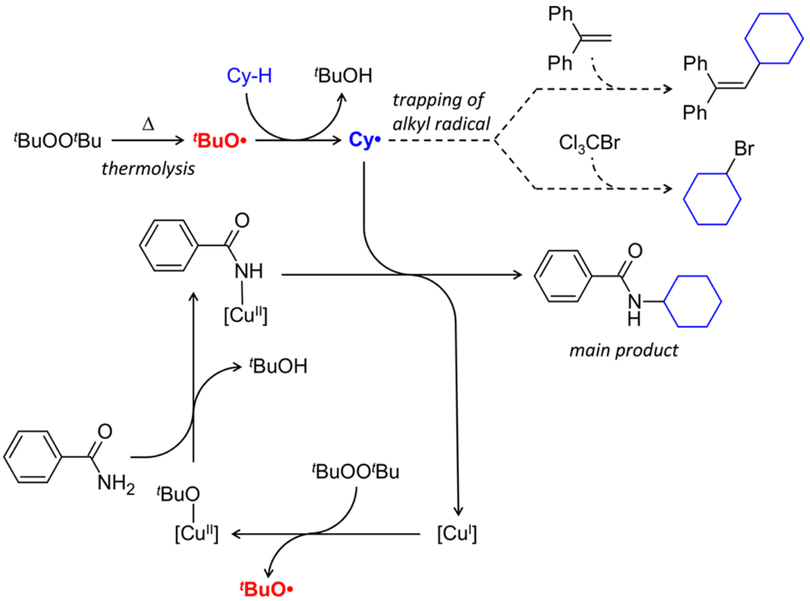

Figure 13. Proposed reaction mechanism for the catalytic cyclohexane amidation system with ᵗBuOOᵗBu as oxidant. Copper complexes **1** and **2** are schematically indicated as [Cu].

between benzamide and chloride, present in **2**, in the reaction with cyclohexyl radical Cy$^\bullet$, which is expected to be one of the main catalytic intermediates (see below). The presence of the methylated byproduct, *N*-methylbenzamide, in the chromatograms (Figure 11) could be explained by the attack of benzamide by methyl radical. The latter is expected to form in low quantities from the ^{t}Bu-O$^\bullet$ radical.[18] Also traces of phenylcyclohexane, presumably formed upon attack of Cy$^\bullet$ to benzene, were observed in all cases.

These results suggested the use of alkyl radical traps, CCl_3Br and 1,1-diphenylethylene,[36,37] to confirm the presence of the cyclohexyl carbon-centered radical. In the competitive reaction with equimolar amounts of benzamide and CCl_3Br (0.5 mmol each), in the presence of the catalyst **2**, bromocyclohexane was observed as the main reaction product, while the formation of all other derivatives of cyclohexane was totally suppressed (Figures 13 and S7). When 1,1-diphenylethylene was applied as a radical trap, no *N*-cyclohexyl benzamide was detected as

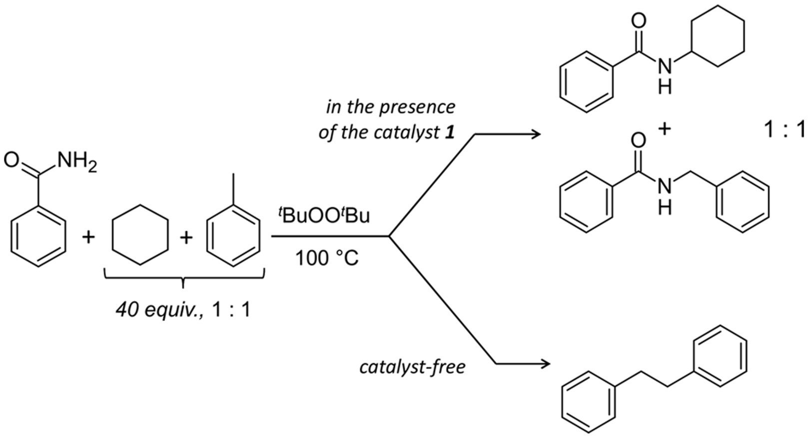

Figure 14. Comparison of the reaction products formed under copper-catalyzed (complex **1**) and catalyst-free conditions.

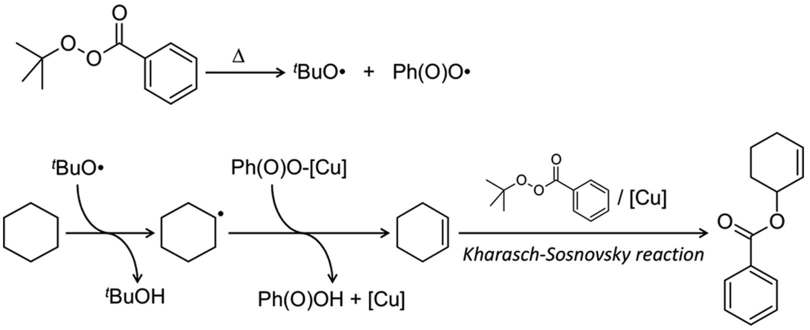

Figure 15. Proposed scheme of allylic ester formation from cyclohexane for the cases of **1**/^{t}BuOO(O)CPh and **2**/^{t}BuOO(O)CPh systems.

well (Figures 13 and S8). Instead, the corresponding trapping products[20] were formed (Figure S8).

The use of benzene solvent was governed by its high inertness toward attack by the ^{t}Bu-O$^\bullet$ radical, which is a proposed C−H attacking species (see below). We attempted to replace benzene with other high-boiling solvents, such as toluene, *α*,*α*,*α*-trifluorotoluene, and chlorobenzene. The comparative reactions were done using equimolar amounts of cyclohexane and solvent (10 mmol each) in order to evaluate the reactivity of each solvent toward the ^{t}Bu-O$^\bullet$ radical relatively to cyclohexane. All the catalytic systems produced *N*-cyclohexylbenzamide as the main reaction product, except with toluene, for which equal amounts of *N*-cyclohexyl- and *N*-benzyl-benzamides were formed (Figure S10). Bibenzyl byproduct was also detected for the case of toluene. For *α*,*α*,*α*-trifluorotoluene, no products attributable to its derivatives were detected, while toluene and chlorobenzene resulted in small amounts of the cross-coupling products of the solvent and cyclohexane (Figure S10). The levels of *N*-methylbenzamide byproduct were much higher for all three solvents in comparison with benzene (Figure S10). It is known that benzene reacts with $CH_3^\bullet$ and ^{t}Bu-O$^\bullet$ radicals in drastically different ways.[38,39] It was proposed that, in the present case, benzene is relatively unreactive toward the ^{t}Bu-O$^\bullet$ radical but acts as a scavenger of the $CH_3^\bullet$ radicals, in this manner reducing the yield of the *N*-methylbenzamide byproduct. The presence of toluene, as a product of benzene methylation, was proved by GC analysis (Figure S12). Interestingly, methylcyclohexane was detected at only trace levels (Figure S12). Further, only negligible amounts of methylated products were found in the cases of the other solvents (Figure S13).

A blank test was performed to clarify if the copper catalyst is required for splitting of the ^{t}BuOO^{t}Bu oxidant and for the formation of the amidation product. Toluene was used as a solvent, for which the appearance of bibenzyl could serve as a marker for a free-radical process. As described above, the process catalyzed by **1** afforded *N*-cyclohexyl and *N*-benzylbenzamides as products. However, in the absence of the catalyst, bibenzyl was formed as a single product (Figure 14), while the *N*-benzylbenzamide was detected only at trace level and *N*-cyclohexylbenzamide was not detected at all (Figure S14). The appearance of bibenzyl (Figure 14) can be understood as a result of the coupling of two benzyl radicals, known to be relatively stable due to the resonance stabilization. Hence, assuming that benzyl radicals originate from the ^{t}Bu-O$^\bullet$ radical attack to toluene, one can conclude that, under the conditions of the experiment, the ^{t}BuOO^{t}Bu oxidant generates ^{t}Bu-O$^\bullet$ radicals in a noncatalytic pathway (Figure 13).

From these observations, as well as from previous reports,[18] one may assume a free radical reaction mechanism with O-centered ^{t}Bu-O$^\bullet$ radical as the main C−H attacking species. The reaction starts with thermolysis of the oxidant to produce the ^{t}Bu-O$^\bullet$ radical (Figure 12). This species is capable of abstracting the hydrogen atom from a C−H bond of cyclohexane[40] to form the alkyl radical (Cy$^\bullet$), which reacts with benzamide activated by coordination to copper (Figure 13). We tried to react **1** and **2** with benzamide to obtain compounds that could be related to the catalytic intermediates, but these attempts were unsuccessful (see the Supporting Information).

We attempted to use acetonitrile and cyclohexane (solvent-free system) solvents but did detect the desired product (*N*-

Table 3. Crystallographic Data for **1** and **2**

	compound			
	1	**2a**	**2b**	**2c**
chemical formula	$C_{20}H_{42}Cu_2N_2O_8$	$C_{16}H_{37}Cl_2Cu_2N_2O_{4.50}$	$C_{16}H_{37}Cl_2Cu_2N_2O_{4.50}$	$C_{16}H_{36.08}Cl_2Cu_2N_2O_{4.04}$
formula mass	565.63	527.45	527.45	519.19
crystal system	monoclinic	monoclinic	monoclinic	monoclinic
a/Å	8.2245(10)	17.9978(19)	17.9899(6)	17.9777(8)
b/Å	8.5718(10)	14.449(2)	14.4314(4)	14.4447(8)
c/Å	17.369(2)	19.249(2)	19.2451(7)	19.3836(10)
α/°	90	90	90	90
β/°	93.384(6)	113.161(6)	113.2170(10)	112.739(2)
γ/°	90	90	90	90
unit cell volume/$Å^3$	1222.3(2)	4602.2(10)	4591.8(3)	4642.3(4)
temperature/K	150(2)	150(2)	150(2)	296(2)
space group	$P2_1/n$	$P2/c$	$P2/c$	$P2/c$
no. of formula units per unit cell, Z	2	8	8	8
reflns measured	12 475	24 165	33 597	69 088
reflns independent	3734	7134	9409	9511
R_{int}	0.0335	0.0860	0.0759	0.0643
final R_1 values ($I > 2\sigma(I)$)	0.0363	0.0472	0.0427	0.0312
final $wR(F^2)$ values (all data)	0.0897	0.1074	0.1009	0.0784
GoF on F^2	1.030	1.018	1.059	1.046
CCDC no.	1487157	1590488	1590489	1487156

cyclohexylbenzamide) even at a trace level, particularly because these solvents do not allow the use of temperatures higher than 80 °C, which is not sufficient for thermal splitting of ^{t}BuOO^{t}Bu.

Replacement of ^{t}BuOO^{t}Bu by ^{t}BuOOH resulted in complete suppression of the desired product formation for both **1** and **2** catalysts. Instead, elevated amounts of cyclohexanol and cyclohexanone were seen (Figure 12), although *N*-methylbenzamide was still detectable.

With ^{t}BuOO(O)Ph as oxidant, the catalytic pathway was considerably different from that for ^{t}BuOO^{t}Bu. While only traces of *N*-cyclohexylbenzamide were seen to arise after 24 h reaction time with ^{t}BuOO(O)Ph oxidant, the allylic ester (cyclohex-2-en-1-yl benzoate) was found as the main reaction product (Figure 12). The conversion of benzamide in this case was lower than 5%, showing that the source of benzoyl group in the ester comes from the oxidant, ^{t}BuOO(O)Ph, but not benzamide, which remains unreacted. From this fact, and also from the observation of cyclohexene as a reaction byproduct (appears close to the cyclohexane peak, not shown in Figure 12), one may suppose that oxidative dehydrogenation of cyclohexane occurs to produce cyclohexene, which then reacts with ^{t}BuOO(O)Ph to form the final allylic ester (Figure 15) in a copper-catalyzed process, known as the Kharasch−Sosnovsky reaction.[41−43] There are a few general mechanisms of mild dehydrogenation of alkanes, such as organometallic dehydrogenation, enzymatic desaturation, and cooperative hydrogen atom transfer.[44] The catalytic systems **1**/^{t}BuOO(O)Ph and **2**/^{t}BuOO(O)Ph probably operate via the last route,[45] where the initial hydrogen abstraction occurs via attack of ^{t}Bu-O$^\bullet$ radical and then the cyclohexyl radical reacts with coordinated benzoate (Figure 15) to form benzoic acid (observed by GC, Figure 12) and cyclohexene. The latter is transformed to allylic ester by means of the Kharasch−Sosnovsky reaction, catalyzed by **1** or **2**. Since no cyclohexene was detected with ^{t}BuOO^{t}Bu or ^{t}BuOOH oxidants, one may conclude that the presence of both ^{t}Bu-O$^\bullet$ and PhC(O)O$^\bullet$ is essential for the dehydrogenation process, which thus can be classified as a cooperative hydrogen atom transfer.[44]

■ CONCLUSIONS

In summary, we have successfully prepared novel coordination compounds, $[Cu_2(H^tBuDea)_2(OAc)_2]$ (**1**) and $[Cu_2(H^nBuDea)_2Cl_2]\cdot nH_2O$ (**2**). The structures of **1** and **2** reveal different supramolecular organizations: in the complex **1** the Cu_2 cores form a H-bonded chain, while in the case of **2** the Cu_2 dimers are joined into supramolecular tetrametallic units which either form H-bonded polymeric chains involving solvent water molecules or remain isolated. The idea of using the bulky aliphatic substituents (^{n}Bu and ^{t}Bu) in the aminoalcohol ligands in the synthesis was to stimulate formation of compounds with discrete polynuclear molecular structures surrounded by bulky moieties, in contrast to the formation of extended polymeric structures. Moreover, the presence of these aliphatic substituents increases the solubility in aprotic nonpolar solvents, which is of great importance for catalytic applications. In the present case, the utilization of this strategy afforded the isolation of **1** and **2**, showing a good solubility in benzene, and their successful application in the above catalytic reaction.

The magnetic investigations of **1** disclosed an antiferromagnetic coupling between copper centers, which can be fitted with the Bleaney−Bowers model. HF-EPR spectroscopy confirmed the presence of magnetically coupled spins $^1/_2$ in the solid state as well as in solution. In contrast to **1**, the magnetic properties of **2** could not be interpreted with this model, showing a significant deviation at low temperatures. Careful analysis of the crystal structure of **2** revealed the presence of four geometrically different dicopper units, joined into two different tetrametallic aggregates. This must result in a superposition of magnetism due to four individual Cu−Cu coupled pairs, or to two different tetranuclear units. Moreover, the Cu−O−Cu angles in these pairs are close to the borderline separating ferromagnetic and antiferromagnetic interactions in copper dinuclear systems. DFT calculations of the magnetic couplings, performed for the structures **2a** and **2c**, predicted that J_{CuCu} constants may vary from antiferro- (110 cm^{-1}) to ferromagnetic (−32 cm^{-1}) couplings.

Furthermore, complexes **1** and **2** act as catalysts for oxidative amidation of cyclohexane with benzamide, showing a moderate activity in the case of the **1**/$^tBuOO^tBu$ system (20% of benzamide conversion). From the experiments with radical traps and various solvents, a free radical main reaction pathway is proposed.

We expect that the results obtained within the present research would improve the understanding of magnetic interactions in spin-coupled systems as well as the exploration of alkane functionalization catalytic processes. These results facilitate further synthesis and investigation of polynuclear coordination compounds with aliphatic-substituted aminoalcohols as novel magnetic and catalytic materials.

■ EXPERIMENTAL SECTION

All chemicals were of reagent grade and used as received. All experiments were carried out in air. Elemental analyses for CHNS were provided by the Microanalytical Service of the Instituto Superior Técnico. Infrared spectra (4000−400 cm^{-1}) were recorded using a PerkinElmer BX-FT IR instrument with KBr pellets.

Synthesis of $[Cu_2(H^tBuDea)_2(OAc)_2]$ (1). $Cu(OAc)_2\cdot H_2O$ (0.5 g, 2.5 mmol) and *N*-*tert*-butyldiethanolamine (0.81 g, 5 mmol) were dissolved in CH_3OH (20 mL), forming a blue-green solution which was magnetically stirred at 50−60 °C (40 min). Precipitation occurred immediately after the start of the reaction. The resulting mixture was filtered off, and the filtrate was kept at room temperature. Light-blue crystals suitable for X-ray crystallographic study were formed from the filtrate in 2 days. Yield: 0.6 g (85%). Anal. Calcd for $C_{20}H_{42}Cu_2N_2O_8$ (*M* = 565.63): C, 42.47; N, 4.95; H, 7.50. Found: C, 42.6; N, 4.8; H, 7.8.

Synthesis of $[Cu_2(H^nBuDea)_2Cl_2]\cdot nH_2O$ (2). $CuCl_2\cdot 2H_2O$ (0.43 g, 2.5 mmol) and *N*-butyldiethanolamine (0.83 g, 5 mmol) were dissolved in CH_3OH (20 mL), forming a blue-green solution which was magnetically stirred at 50−60 °C (120 min). Precipitation occurred immediately after the start of the reaction, but the precipitate was completely dissolved after 1 h of reaction. The resulting solution was filtered, and green crystals suitable for X-ray crystallographic study were formed in 1 day. Yield: 0.25 g (39%). Anal. Calcd for **2a** and **2b** (n = 0.5): $C_{16}H_{37}Cl_2Cu_2N_2O_{4.50}$ (*M* = 527.45): C, 36.43; N, 5.31; H, 7.09%. Found: C, 36.5; N, 5.2; H, 7.2%. Anal. Calcd for **2c** (n = 0.037): $C_{16}H_{36.08}Cl_2Cu_2N_2O_{4.04}$ (*M* = 519.19): C, 37.01; N, 5.40; H, 7.02%. Found: C, 37.1; N, 5.4; H, 7.0%.

Crystallography. The X-ray diffraction data for **1** and **2** were collected using a Bruker AXS KAPPA APEX II diffractometer with graphite-monochromated Mo K*α* radiation (Table 3). Data were collected using omega scans of 0.5° per frame, and a full sphere of data was obtained. Cell parameters were retrieved using Bruker SMART software and refined using Bruker SAINT on all the observed reflections. Absorption corrections were applied using SADABS.[46] The structures were solved by direct methods and refined against F^2 using the programs SHELX-2014 (for **1**) or SHELX-2016/6 (for **2**).[47]

The hydrogen atoms H2 (in **1**) and H1−H4 (in **2**) were located in a difference Fourier map and refined with O−H distance restrained to 0.85 Å (for **2a**) or refined freely (in all other cases). The positions of the H1W and H2W hydrogen atoms of the uncoordinated water molecules in all structures of **2** were calculated on the basis of geometry and force-field considerations using the CALC-OH program[48] within the WinGX package[49] and not refined. All the other hydrogen atoms in all the structures were placed at calculated positions and refined using the model with $U_{iso} = nU_{eq}$ (n = 1.5 for H atoms of methyl group and water H atoms, and n = 1.2 for methylenic H atoms).

The first X-ray data set for compound **2** (**2a**) was occasionally collected with low completeness of 0.778, although the quality of the data was sufficiently high for successful solution and refinement of the structure (Table 3). The X-ray experiment was repeated resulting in the crystal structure **2b**, having full completeness. However, the quality of the data **2b** was not sufficient for full refinement of the H atoms on the O—H···O bonds. Thus, the data set **2c** was collected from the other sample of **2** and using greater redundancy (69 088 reflections against 33 597 for **2b**, Table 3), finally allowing us to obtain the most precise data for the H-bonding structure (Table 1).

The difference peaks in the Fourier maps that correspond to the water molecules O1W have intensities of 5.92, 6.66, and 0.63 e Å^{-3} for **2a**, **2b**, and **2c**, respectively. Considering a very low intensity in the case of **2c** and also the elemental analysis data, the occupancy of the water molecule in **2c** was refined to be 0.073(7) (this number is per four copper atoms).

Magnetic Measurements. Magnetic susceptibility data of powdered samples were measured with a SQUID magnetometer (Quantum Design MPMSXL-5) over the temperature range 1.8−300 K at a magnetic induction of 0.5 T. Corrections for the sample holders were applied. Diamagnetic corrections for the molecules were determined from Pascal's constants.[50]

HF-EPR Spectroscopy. High-frequency EPR spectra were recorded with a home-built spectrometer at the EMR facility of NHMFL. The instrument is a transmission-type device in which waves are propagated in cylindrical light-pipes. The microwaves were generated by a phase-locked oscillator (Virginia Diodes) operating at a frequency of 13 ± 1 GHz and generating its harmonics, of which the 4th, 8th, 12th, 16th, 24th, and 32nd were available. A superconducting magnet (Oxford Instruments) capable of reaching a field of 17 T was employed.

Thermogravimetric Measurements. A PerkinElmer STA-6000 model thermogravimetric analyzer was used for determination of the thermal stability of complexes **1** and **2** (Figure S15). Samples weighing ca. 10 mg were heated from 30 to 1000 °C at a heating rate of 1−10 °C min^{-1} under N_2 atmosphere.

Catalytic Reactions. The reactions were typically carried out under N_2 atmosphere in a thermostated Schlenk tube under vigorous stirring. First the catalyst (12.5 μmol, 7 and 6.5 mg for **1** and **2**, respectively) and benzamide (0.5 mmol, 60.6 mg) were introduced into the tube in the solid form. Next benzene (1 mL) and cyclohexane (5 mmol, 0.54 mL) were added in that order. The oxidant (1 mmol) $^tBuOO^tBu$, ^tBuOOH (70% aq), or $^tBuOO(O)CPh$ (184, 138, and 190 μL, respectively) was then added at room temperature, and the mixture was immediately frozen with liquid nitrogen. The gas atmosphere was pumped and filled with N_2 a few times in order to remove air. The frozen mixture was left to warm up under vacuum (to degasify) until becoming a liquid, and the above procedure was repeated. Finally the Schlenk tube was filled with N_2, and the reaction mixture was heated at 90 °C for 24 h with a possibility of gas escape to compensate excessive pressure. The reaction mixtures were cooled to room temperature, 10 mL of CH_3CN and 100 μL of *α*,*α*,*α*-trifluorotoluene or 2,2,4-trimethylpentane (GC standard) were added, and the resulting mixture was directly analyzed by GC/GC-MS techniques.

Gas Chromatography. A PerkinElmer Clarus 600 gas chromatograph, equipped with two nonpolar capillary columns (SGE BPX5; 30 m × 0.22 mm × 25 μm), one having an EI-MS (electron impact) detector and the other one with a FID detector, was used for analyses of the reaction mixtures. The following GC conditions were applied: 50 °C (3 min), 50−150 °C (30° per minute), 150−300 °C (14° per minute), 300 °C (4.95 min), 20 min total run time; 200 °C injector temperature. Helium was used as the carrier gas (1 mL per minute constant flow). All EI mass spectra were recorded with 70 eV energy. The identification of peaks on the chromatograms was made on the basis of comparison of respective EI mass spectra with those from the NIST database v. 2.2 (PerkinElmer TurboMass v. 5.4.2.1617 software was used).

DFT Calculations. "Broken symmetry"[51−53] Density Functional Theory calculations were performed by using the software ORCA[54,55] to get insight into the mechanism of the exchange interactions. In this method, a self-consistent-field (SCF) calculation is first performed for the $S = 1$ spin state of a dinuclear copper complex. Next, a "broken symmetry" state is set up, with the unpaired electron being spin-up on one copper ion and spin-down on the other, and another SCF calculation is performed. The energies of the high-spin and broken symmetry states are finally used to estimate the exchange integral value, J (for Hamiltonian $\hat{\mathbf{H}} = J\ \hat{\mathbf{S}}_1 \cdot \hat{\mathbf{S}}_2$), based on the equation $J = 2(E_{HS} - E_{BS})/(\langle S^2 \rangle_{HS} - \langle S^2 \rangle_{BS})$, where E_{HS} and E_{BS} are the energies of the high-spin (HS) and the broken-symmetry (BS) states and $\langle S \rangle^2$ are the expectation values of the spin-squared operator in the HS and BS states. The equation is adapted to the $+J\mathbf{S}_1 \cdot \mathbf{S}_2$ convention used in this paper. The original equation used in the ORCA program is $J = -(E_{HS} - E_{BS})/(\langle S^2 \rangle_{HS} - \langle S^2 \rangle_{BS})$, since ORCA uses the Hamiltonian $-2J\mathbf{S}_1 \cdot \mathbf{S}_2$. Ahlrichs-type basis set TZVPP for the metal and all coordinated atoms and SVP for other atoms were used, combined with the B3LYP functional.[56−59] Ahlrichs polarization functions from basis H-Kr R and auxiliary bases from the TurboMole library were also used.[60,61]

The X-ray atom coordinates were used in calculations. The J value of 230 cm^{-1} was obtained here from a formula converting the energy difference between the HS and the BS states, which is referred to in the literature as "spin-projected"[51−53] and should be good for strong exchange interactions. The "non-spin-projected" formula results in 2 times smaller J, much closer to the experimental result. There have been discussions among experts regarding which approach should be used.[51−53] In recent papers by some of us dealing with single-atom-bridged copper complexes, we have used the "spin-projected" J values, which were obtained typically ∼30% larger than the experimental values; thus, the present result is rather disappointing.

■ ASSOCIATED CONTENT

Ⓢ Supporting Information

The Supporting Information is available free of charge on the ACS Publications website at DOI: 10.1021/acs.inorgchem.8b02145.

> Figures S1−S15 and Tables S1−S3, showing IR spectra, bond distances and angles, polyhedral representations, molar magnetic susceptibility plots, powder X-ray, GC-MS, and GC-FID chromatograms, EI-MS spectra, and thermogravimetric plots; discussion of the simulation of the pair of dimers spectra; and experimental details for reactions of **1** and **2** with benzamide in toluene (PDF)

Accession Codes

CCDC 1487156,1487157, 1590488, and 1590489 contain the supplementary crystallographic data for this paper. These data can be obtained free of charge via www.ccdc.cam.ac.uk/data_request/cif, or by emailing data_request@ccdc.cam.ac.uk, or by contacting The Cambridge Crystallographic Data Centre, 12 Union Road, Cambridge CB2 1EZ, UK; fax: +44 1223 336033.

■ AUTHOR INFORMATION

Corresponding Authors

*E-mail: dmytro.nesterov@tecnico.ulisboa.pt.
*E-mail: pombeiro@tecnico.ulisboa.pt.

ORCID

Oksana V. Nesterova: 0000-0002-0114-6525
Dmytro S. Nesterov: 0000-0002-1095-6888
Andrew Ozarowski: 0000-0001-6225-9796

Notes

The authors declare no competing financial interest.

■ ACKNOWLEDGMENTS

This work was supported by Fundação para a Ciência e Tecnologia (FCT), Portugal (projects PTDC/QEQ-QIN/3967/2014 and UID/QUI/00100/2013; fellowships SFRH/BPD/63710/2009 (O.V.N.) and SFRH/BPD/99533/2014 (D.S.N.)). The high-field EPR spectra were recorded at the NHMFL, which is funded by the NSF through the Cooperative Agreement No. DMR-1157490 and the State of Florida. J.J. is grateful to the Ministry of Science and Higher Education of the Polish Republic for financial support in her statutory activities of the Faculty of Chemistry of Wroclaw University and for the purchase of the SQUID magnetometer.

■ REFERENCES

(1) Nesterov, D. S.; Nesterova, O. V.; Pombeiro, A. J. L. Homo- and heterometallic polynuclear transition metal catalysts for alkane C-H bonds oxidative functionalization: Recent advances. *Coord. Chem. Rev.* **2018**, *355*, 199−222.

(2) Sharples, J. W.; Collison, D. The coordination chemistry and magnetism of some 3d-4f and 4f amino-polyalcohol compounds. *Coord. Chem. Rev.* **2014**, *260*, 1−20.

(3) Nesterov, D. S.; Nesterova, O. V.; Kokozay, V. N.; Pombeiro, A. J. L. Polynuclear Heterometallic Complexes from Metal Powders: The "Direct Synthesis" Approach. *Eur. J. Inorg. Chem.* **2014**, *2014*, 4496−4517.

(4) Papatriantafyllopoulou, C.; Moushi, E. E.; Christou, G.; Tasiopoulos, A. J. Filling the gap between the quantum and classical worlds of nanoscale magnetism: giant molecular aggregates based on paramagnetic 3d metal ions. *Chem. Soc. Rev.* **2016**, *45*, 1597−1628.

(5) Ardizzoia, G. A.; Brenna, S. Hydroxo-bridged copper(II) cubane complexes. *Coord. Chem. Rev.* **2016**, *311*, 53−74.

(6) The Cambridge Structural Database (v. 5.38, May 2017) contains 560 structures with diethanolamine and its derivatives.

(7) Nesterov, D. S.; Jezierska, J.; Nesterova, O. V.; Pombeiro, A. J. L.; Ozarowski, A. An unprecedented octanuclear copper core with *C3i* symmetry and a paramagnetic ground state. *Chem. Commun.* **2014**, *50*, 3431−3434.

(8) Nesterov, D. S.; Alegria, E. C. B. A.; Jezierska, J. A new member of Cu_8(II) family: Synthesis, structure and magnetic properties of an octanuclear copper complex with N-*tert*-butyldiethanolamine. *Inorg. Chim. Acta* **2017**, *460*, 83−88.

(9) Kirillov, A. M.; Kirillova, M. V.; Pombeiro, A. J. L. Multicopper complexes and coordination polymers for mild oxidative functionalization of alkanes. *Coord. Chem. Rev.* **2012**, *256*, 2741−2759.

(10) Elwell, C. E.; Gagnon, N. L.; Neisen, B. D.; Dhar, D.; Spaeth, A. D.; Yee, G. M.; Tolman, W. B. Copper-Oxygen Complexes Revisited: Structures, Spectroscopy, and Reactivity. *Chem. Rev.* **2017**, *117*, 2059−2107.

(11) Hong, S.; Lee, Y. M.; Ray, K.; Nam, W. Dioxygen activation chemistry by synthetic mononuclear nonheme iron, copper and chromium complexes. *Coord. Chem. Rev.* **2017**, *334*, 25−42.

(12) Lazreg, F.; Nahra, F.; Cazin, C. S. J. Copper-NHC complexes in catalysis. *Coord. Chem. Rev.* **2015**, *293*, 48−79.

(13) Wang, V. C. C.; Maji, S.; Chen, P. R. Y.; Lee, H. K.; Yu, S. S. F.; Chan, S. I. Alkane Oxidation: Methane Monooxygenases, Related Enzymes, and Their Biomimetics. *Chem. Rev.* **2017**, *117*, 8574−8621.

(14) Zhang, S.; Li, Y. A.; Xu, Y. G.; Wang, Z. Y. Recent progress in copper catalyzed asymmetric Henry reaction. *Chin. Chem. Lett.* **2018**, *29*, 873−883.

(15) Gao, M. C.; Ye, R. X.; Shen, W. J.; Xu, B. Copper nitrate: a privileged reagent for organic synthesis. *Org. Biomol. Chem.* **2018**, *16*, 2602−2618.

(16) Wang, S.; Du, G. X.; Xi, C. J. Copper-catalyzed carboxylation reactions using carbon dioxide. *Org. Biomol. Chem.* **2016**, *14*, 3666−3676.

(17) Studer, A.; Curran, D. P. Catalysis of Radical Reactions: A Radical Chemistry Perspective. *Angew. Chem., Int. Ed.* **2016**, *55*, 58−102.

(18) Tran, B. L.; Li, B. J.; Driess, M.; Hartwig, J. F. Copper-Catalyzed Intermolecular Amidation and Imidation of Unactivated Alkanes. *J. Am. Chem. Soc.* **2014**, *136*, 2555−2563.

(19) Gephart, R. T.; Huang, D. L.; Aguila, M. J. B.; Schmidt, G.; Shahu, A.; Warren, T. H. Catalytic C?H Amination with Aromatic Amines. *Angew. Chem., Int. Ed.* **2012**, *51*, 6488−6492.

(20) Liu, D.; Li, Y. X.; Qi, X. T.; Liu, C.; Lan, Y.; Lei, A. W. Nickel-Catalyzed Selective Oxidative Radical Cross-Coupling: An Effective Strategy for Inert Csp^3-H Functionalization. *Org. Lett.* **2015**, *17*, 998−1001.

(21) Yang, H. L.; Sun, P.; Zhu, Y.; Yan, H.; Lu, L. H.; Qu, X. M.; Li, T. Y.; Mao, J. C. Copper-catalyzed decarboxylative Csp^2-Csp^3 coupling reactions via radical mechanism. *Chem. Commun.* **2012**, *48*, 7847−7849.

(22) Zhao, J. C.; Fang, H.; Han, J. L.; Pan, Y. Iron-catalyzed decarboxylative alkenylation of cycloalkanes with arylvinyl carboxylic acids via a radical process. *Beilstein J. Org. Chem.* **2013**, *9*, 1718−1723.

(23) Zeng, H. T.; Huang, J. M. Copper-Catalyzed Ligand-Free Amidation of Benzylic Hydrocarbons and Inactive Aliphatic Alkanes. *Org. Lett.* **2015**, *17*, 4276−4279.

(24) Nakamoto, K. Infrared and Raman Spectra of Inorganic and Coordination Compounds: Part A: Theory and Applications. In *Inorganic Chemistry*, 6th ed.; Wiley, 2009.

(25) Deacon, G. B.; Phillips, R. J. Relationships between the carbon-oxygen stretching frequencies of carboxylato complexes and the type of carboxylate coordination. *Coord. Chem. Rev.* **1980**, *33*, 227−250.

(26) Mazus, M. D.; Kovalennko, A. L.; Simonov, Y. A.; Polyakov, V. N. Structure of the dimeric copper(II) complex with 2-hydroxyethyl-(n-propyl)-amine. *Zh. Neorg. Khim.* **1987**, *32*, 2718−2722.

(27) Hay, P. J.; Thibeault, J. C.; Hoffmann, R. Orbital interactions in metal dimer complexes. *J. Am. Chem. Soc.* **1975**, *97*, 4884−4899.

(28) Ozarowski, A.; Calzado, C. J.; Sharma, R. P.; Kumar, S.; Jezierska, J.; Angeli, C.; Spizzo, F.; Ferretti, V. Metal-Metal Interactions in Trinuclear Copper(II) Complexes [$Cu_3(RCOO)_4(H_2TEA)_2$] and Binuclear [$Cu_2(RCOO)_2(H_2TEA)_2$]. Syntheses and Combined Structural, Magnetic, High-Field Electron Paramagnetic Resonance, and Theoretical Studies. *Inorg. Chem.* **2015**, *54*, 11916−11934.

(29) Sharma, R. P.; Saini, A.; Monga, D.; Venugopalan, P.; Jezierska, J.; Ozarowski, A.; Ferretti, V. Influence of nitrogen donor ligands on the coordination modes of copper(II) 2-nitrobenzoate complexes: structures, DFT calculations and magnetic properties. *New J. Chem.* **2014**, *38*, 437−447.

(30) Maurice, R.; Sivalingam, K.; Ganyushin, D.; Guihery, N.; de Graaf, C.; Neese, F. Theoretical Determination of the Zero-Field Splitting in Copper Acetate Monohydrate. *Inorg. Chem.* **2011**, *50*, 6229−6236.

(31) Singh, S. K.; Rajaraman, G. Probing the Origin of Magnetic Anisotropy in a Dinuclear {Mn^{III}Cu^{II}} Single- Molecule Magnet: The Role of Exchange Anisotropy. *Chem. - Eur. J.* **2014**, *20*, 5214−5218.

(32) Atanasov, M.; Comba, P.; Hanson, G. R.; Hausberg, S.; Helmle, S.; Wadepohl, H. Cyano-bridged Homodinuclear Copper(II) Complexes. *Inorg. Chem.* **2011**, *50*, 6890−6901.

(33) Ozarowski, A.; Reinen, D. Anisotropic Exchange Interactions in the Copper(II) and Vanadium(IV) Dimers [(L')Cu(μ-OH)$_2$Cu(L')]-(ClO_4)$_2$ and [(L)VO(μ-OH)$_2$VO(L)]Br$_2$ with 1,4,7-Triazacyclononane (L) and Its N,N',N''-Trimethyl Derivative (L') - a Single-Crystal Electron-Paramagnetic-Res Stud. *Inorg. Chem.* **1986**, *25*, 1704−1708.

(34) Ozarowski, A.; Szymanska, I. B.; Muziol, T.; Jezierska, J. High-Field EPR and Magnetic Susceptibility Studies on Binuclear and Tetranuclear Copper Trifluoroacetate Complexes. X-ray Structure Determination of Three Tetranuclear Quinoline Adducts of Copper-(II) Trifluoroacetate. *J. Am. Chem. Soc.* **2009**, *131*, 10279−10292.

(35) Crawford, V. H.; Richardson, H. W.; Wasson, J. R.; Hodgson, D. J.; Hatfield, W. E. Relationship between singlet-triplet splitting and Cu-O-Cu bridge angle in hydroxo-bridged copper dimers. *Inorg. Chem.* **1976**, *15*, 2107−2110.

(36) Fokin, A. A.; Schreiner, P. R. Selective alkane transformations via radicals and radical cations: Insights into the activation step from experiment and theory. *Chem. Rev.* **2002**, *102*, 1551−1593.

(37) Giese, B. Formation of cc bonds by addition of free-radicals to alkenes. *Angew. Chem., Int. Ed. Engl.* **1983**, *22*, 753−764.

(38) Brook, J. H. T.; Snedden, W. Reaction of methyl + t-butoxy radicals with benzene. *Tetrahedron* **1964**, *20*, 1043−1050.

(39) Levy, M.; Steinberg, M.; Szwarc, M. The addition of methyl radicals to benzene. *J. Am. Chem. Soc.* **1954**, *76*, 3439−3441.

(40) MacFaul, P. A.; Ingold, K. U.; Wayner, D. D. M.; Que, L. A putative monooxygenase mimic which functions via well-disguised free radical chemistry. *J. Am. Chem. Soc.* **1997**, *119*, 10594−10598.

(41) Kharasch, M. S.; Sosnovsky, G. The reactions of *tert*-butyl perbenzoate and olefins - a stereospecific reaction. *J. Am. Chem. Soc.* **1958**, *80*, 756−756.

(42) Sekar, G.; DattaGupta, A.; Singh, V. K. Asymmetric Kharasch reaction: Catalytic enantioselective allylic oxidation of olefins using chiral pyridine bis(diphenyloxazoline) copper complexes and *tert*-butyl perbenzoate. *J. Org. Chem.* **1998**, *63*, 2961−2967.

(43) Mayoral, J. A.; Rodriguez-Rodriguez, S.; Salvatella, L. Theoretical Insights into Enantioselective Catalysis: The Mechanism of the Kharasch-Sosnovsky Reaction. *Chem. - Eur. J.* **2008**, *14*, 9274−9285.

(44) West, J. G.; Huang, D.; Sorensen, E. J. Acceptorless dehydrogenation of small molecules through cooperative base metal catalysis. *Nat. Commun.* **2015**, *6*.10093

(45) Tran, B. L.; Driess, M.; Hartwig, J. F. Copper-Catalyzed Oxidative Dehydrogenative Carboxylation of Unactivated Alkanes to Allylic Esters via Alkenes. *J. Am. Chem. Soc.* **2014**, *136*, 17292−17301.

(46) Bruker. *APEX2 & SAINT*; AXS Inc.: Madison, WI, 2004.

(47) Sheldrick, G. M. Crystal structure refinement with SHELXL. *Acta Crystallogr., Sect. C: Struct. Chem.* **2015**, *71*, 3−8.

(48) Nardelli, M. Modeling hydroxyl and water H atoms. *J. Appl. Crystallogr.* **1999**, *32*, 563−571.

(49) Farrugia, L. J. WinGX and ORTEP for Windows: an update. *J. Appl. Crystallogr.* **2012**, *45*, 849−854.

(50) Bain, G. A.; Berry, J. F. Diamagnetic corrections and Pascal's constants. *J. Chem. Educ.* **2008**, *85*, 532−536.

(51) Malrieu, J. P.; Caballol, R.; Calzado, C. J.; de Graaf, C.; Guihery, N. Magnetic Interactions in Molecules and Highly Correlated Materials: Physical Content, Analytical Derivation, and Rigorous Extraction of Magnetic Hamiltonians. *Chem. Rev.* **2014**, *114*, 429−492.

(52) Ruiz, E.; Cano, J.; Alvarez, S.; Alemany, P. Broken symmetry approach to calculation of exchange coupling constants for homobinuclear and heterobinuclear transition metal complexes. *J. Comput. Chem.* **1999**, *20*, 1391−1400.

(53) Onofrio, N.; Mouesca, J.-M. Analysis of the Singlet-Triplet Splitting Computed by the Density Functional Theory-Broken-Symmetry Method: Is It an Exchange Coupling Constant? *Inorg. Chem.* **2011**, *50*, 5577−5586.

(54) Neese, F. *ORCA*, An ab initio, Density Functional and Semiempirical Program Package, Version 2.9.1, 2012.

(55) Neese, F. The ORCA program system. *Comput. Mol. Sci.* **2012**, *2*, 73−78.

(56) Becke, A. D. Density-functional exchange-energy approximation with correct asymptotic-behavior. *Phys. Rev. A: At., Mol., Opt. Phys.* **1988**, *38*, 3098−3100.

(57) Perdew, J. P. Density-functional approximation for the correlation-energy of the inhomogeneous electron-gas. *Phys. Rev. B: Condens. Matter Mater. Phys.* **1986**, *33*, 8822−8824.

(58) Perdew, J. P. Erratum: Density-Functional Approximation for the Correlation Energy of the Inhomogeneous Electron Gas. *Phys. Rev. B: Condens. Matter Mater. Phys.* **1986**, *34*, 7406−7406.

(59) Kendall, R. A.; Fruchtl, H. A. The impact of the resolution of the identity approximate integral method on modern ab initio algorithm development. *Theor. Chem. Acc.* **1997**, *97*, 158−163.

(60) Schafer, A.; Horn, H.; Ahlrichs, R. Fully optimized contracted gaussian-basis sets for atoms li to kr. *J. Chem. Phys.* **1992**, *97*, 2571−2577.

(61) The Ahlrichs auxiliary basis sets were obtained from the TurboMole basis set library under ftp.chemie.uni-karlsruhe.de/pub/jbasen.